Simultaneously retrieving cloud optical depth and effective radius for optically thin clouds

Qilong Min and Minzheng Duan

Atmospheric Science Research Center, State University of New York, Albany, New York, USA

Received 27 April 2005; revised 1 July 2005; accepted 21 July 2005; published 2 November 2005.

[1] A new technique for simultaneously retrieving cloud optical depth and effective radius has been proposed. This approach is based on the angular distribution of scattered light in the forward scattering lobe of cloud drops. The angular distributions can be observed by multiple shadowband scans. Radiative transfer modeling simulations demonstrate that accuracies for cloud optical depth, effective radius, and liquid water path are 2%, 10%, and 2 gm^{-2}, respectively, for given possible instrument noise and uncertainties. Further, we have tested different measurement strategies and achieved consistent accuracies. This technique will provide an approach to deal with the issue of "CLOWD (cloud with low optical (water) depth)."

Citation: Min, Q., and M. Duan (2005), Simultaneously retrieving cloud optical depth and effective radius for optically thin clouds, *J. Geophys. Res.*, *110*, D21201, doi:10.1029/2005JD006136.

1. Introduction

[2] Aerosols and clouds play key roles in the atmospheric energy balance and in the hydrological cycle. Detailed knowledge of the radiative properties of aerosol and clouds is crucial to obtain further advances in the study of climate change. However, the ability to accurately measure cloud optical properties is limited, particularly for optically thin clouds. Recent assessment of the cloud liquid water path (LWP) measurements at the ARM SGP site concludes that uncertainty in state-of-the-art LWP retrievals using passive microwave radiometer is 20 gm^{-2} with a bias of 15 to 30 gm^{-2} [*Marchand et al.*, 2003]. The relative error is overwhelmed when LWP is small. Furthermore, over 50% of the warm liquid water clouds at the SGP site have LWP less than 100 gm^{-2} with the mode of 40 gm^{-2}. This means that ARM with state-of-the-art instrument suites is still unable to adequately observe over half of the overhead clouds [*Marchand et al.*, 2003].

[3] The radiative impact of clouds is governed by the macrophysical and microphysical properties of the clouds, especially cloud water path and particle size and shape. Both solar and thermal radiation reaching the surface or reflecting back to the space is a nonlinear function of the cloud liquid water. Figure 1 shows dramatic (exponential) changes in shortwave (SW) and longwave (LW) radiation as a function of LWP for a simple plane-parallel case. In this simulation, the solar zenith angle is set to 45 degrees and a cloud layer is placed between 1 and 2 km. The uncertainty of 20 gm^{-2} in the LWP has relatively large radiative impact on SW radiation (over 150 wm^{-2}) when LWP is small. The magnitude of radiation uncertainty strongly depends on the effective radius of clouds: the smaller the effective radius the greater the uncertainty. It illustrates the importance of accurate measurements of both LWP and effective radius. Although LW radiation is insensitive to effective radius of clouds, LW cloud radiative forcing changes significantly with LWP when LWP is small. Furthermore, research on aerosol indirect effect on clouds also needs accurate measurements of LWP and effective radius. Therefore it is vitally important to measure LWP and effective radius accurately and simultaneously, particularly for low-LWP conditions.

[4] Various efforts have been made to derive cloud optical and microphysical properties from visible and infrared radiation measurements, from passive microwave radiometers, and from active measurements from radars and lidars. However, no single sensor has proven to be capable of doing the job for the wide variety of atmospheric cloud situations, particularly retrieving LWP and effective radius for low-LWP clouds. Several retrieval algorithms have been developed to infer cloud optical depth, using narrowband and broadband diffuse measurements for overcast clouds [*Leontieva and Stamnes*, 1996; *Min and Harrison*, 1996; *Dong et al.*, 1997], normalized difference cloud indexes for broken clouds [*Marshak et al.*, 2000; *Barker and Marshak*, 2001], and narrowband spectral direct beam measurements for thin clouds [*Min et al.*, 2004]. All the methods require the microwave radiometer-retrieved LWP as a constraint to derive the effective radius. Those approaches, however, are ineffective for low-LWP clouds or invalid for inhomogeneous scattering clouds because of the limitation of these retrieval methods. As discussed previously, these clouds are among the most common clouds in the atmosphere. Therefore current retrieval methods fail to accurately retrieve a measurable amount of the global cloud optical properties. In general,

0148-0227/05/2005JD006136$09.00

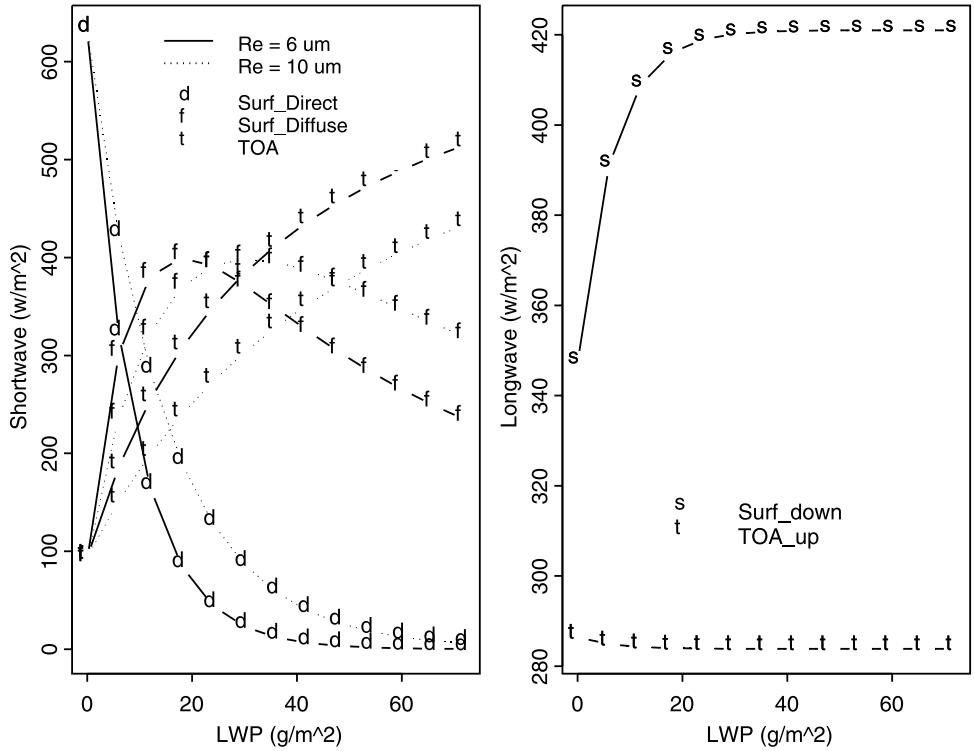

Figure 1. Shortwave and longwave fluxes at both surface and TOA as a function of cloud liquid water path.

lidar systems detect essentially all clouds that are visible from the ground and are within the range of instrument height measurements. However, the laser beams are strongly attenuated by cloud water, limiting lidar detection range of cloud optical depth to $\sim 2-3$. The great strength of radar is its ability to penetrate clouds and reveal multiple layers aloft. The millimeter wave cloud radar, however, fails to detect some of these clouds, especially if the clouds are composed of small hydrometeors, or the clouds may be thinner than the radar sample volume depth resulting in partial beam filling and reduced reflectivity. It is vital to find a means to observe low–liquid water clouds.

[5] To fill the current gaps in accurate small LWP measurement, we propose a new multichannel and multiscan radiometer (MMR) that will simultaneously retrieve cloud optical depth and effective radius. The angular distribution of scattered light in the forward scattering lobe of a particle changes rapidly with its size, but is almost independent of its refractive index. The sizing of particles from the angular distribution of their forward scattering lobe can be traced back to the Eriometer of Thomas Young in 1813. Since then, there have been many applications even for smaller particles in the Mie scattering region. Atmospheric scientists have a long history of inferring aerosol extinction and the single-scattering phase function from measurements of direct and diffuse solar radiation in the solar aureole where brightness is enhanced around the solar disk because of the forward scattering of light by the aerosol particles [*Hodkinson*, 1966; *Nakajima et al.*, 1983; *Kaufman et al.*, 1994; *Dubovik et al.*, 2000]. Here we exploit the possibility to infer the size of liquid water cloud particles and the liquid water path using the solar aureole technique.

2. Forward Scattering Lobe and Particle Size Distribution

2.1. Mie Theory and Phase Function

[6] Radiative intensity of the solar aureole under cloudy conditions is determined via optical properties of clouds, particularly the forward scattering lobe of the single scattering of clouds. Single scattering properties of spherical water cloud particles can be accurately calculated by Mie theory. However, different types of clouds have different total numbers of densities, mean radii, and size distributions, and thus different radiative properties. Many researchers extensively studied the sensitivity of single scattering properties of water clouds to the particle size distribution and found that in many applications cloud optical properties depend primarily on the effective radius, and are insensitive to details of the size distribution such as modality, shape, width, and higher moments [*Hansen and Travis*, 1974; *Hu and Stamnes*, 1993]. The perturbations of cloud optical properties obtained by changing the cloud droplet size distribution for a given cloud liquid water content (associated with cloud concentration) and effective radius are negligible compared with those resulting from changes in the effective radius and liquid water content. This unique dependence of cloud single scattering properties on effective radius and liquid water content provides an important application for simultaneously retrieving cloud droplet effective radius and LWP from the forward scattering lobe

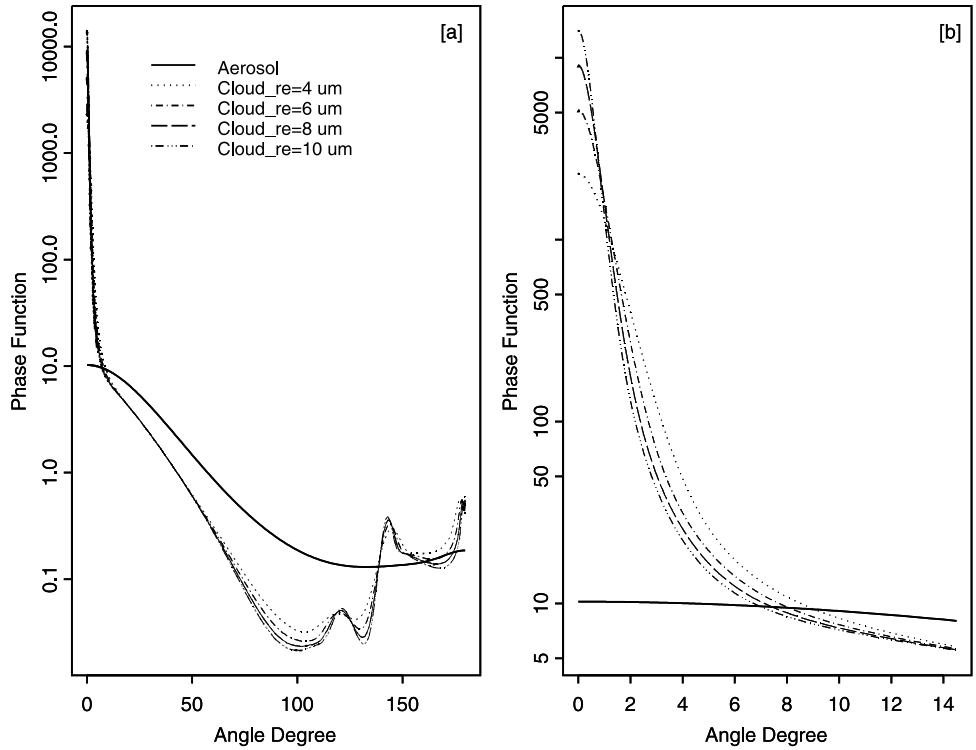

Figure 2. (a and b) Cloud phase functions for different effective radius and aerosol phase functions.

scan. Figure 2 shows phase functions at 415 nm for an effective radius ranging from 4 to 10 μm calculated by Mie theory, and illustrates the fundamental physics for retrieving effective radius from the forward scattering lobe. In the calculations a lognormal distribution with a variance of 0.2 was assumed. Figure 2b is the expansion of Figure 2a for a scattering angle ranging from 0 to 15 degrees, and shows significant differences due to the size of cloud droplets. The large effective radius is always associated with the strong and narrow forward scattering. When the scattering angle approaches 12 degrees the difference is diminished.

2.2. Shadowband Technique

[7] Various techniques have been used to measure solar aureole radiation: tracking sunphotometry, shadowband radiometer, and imaging aureole radiometer [*Harrison et al.*, 1994; *Ritter and Voss*, 2000]. The shadowband method has proven robust for measurement accuracy and long-term deployment [*Min et al.*, 2005]. We propose a multiscan shadowband radiometer that scans across the solar aureole. The shadow band accurately rotates around the polar axis by a microcomputer controlled stepping motor to block a strip of sky, which is sufficient to block the solar disk. The radiance of solar aureole corresponding to the shadowband strip is obtained by differencing the blocked and unblocked irradiances measured by a Lambertian detector. As shadowband rotating around solar aureole, the forward scattering lobe of solar aureole and direct normal irradiance are measured by the radiometer. The advantage of the shadowband technique is that the forward scattering lobe (with direct normal irradiance) and the total horizontal irradiance are simultaneously measured by the same detector. It allows accurate determination of atmospheric transmittances without requiring absolute calibration: Langley regression of the direct normal irradiance with associated forward scattering lobe taken on stable, clear days can be used to extrapolate the instrument's response to the top of the atmosphere (TOA), and this calibration can then be applied to the total horizontal irradiance. Transmittances are calculated subsequently under all-sky conditions as the ratio of the uncalibrated signal to the extrapolated TOA value.

3. Retrieval Algorithm

3.1. Simulation of MMR Measurements and Sensitivity Study

[8] To simulate the MMR measurements requires a forward radiative transfer model that accurately computes the radiation intensity. However, computing the radiation intensity of clouds is very challenging, particularly for the solar aureole region, because of the strong forward peak of the phase function. To represent the δ function-like forward peak feature via the discrete ordinate methods requires a large number of Legendre polynomial terms. The δ-M method, which takes advantage of the fact that the higher-order terms in the Legendre polynomial expansion contribute primarily to the forward peak, truncates the Legendre polynomial to effectively remove the forward peak and has proven to be a most reliable means for flux computations [*Wiscombe*, 1977]. However, if there are insufficient streams in the expansion, the δ-M method results in oscillation of the truncated phase function and causes problems for radiance computations in both forward and backward directions. *Min et al.* [2004] developed a radiative transfer model based on the DISORT [*Stamnes et al.*, 1988] that can yield the intensity field with an error of less that 1% by combining the δ-fit method [*Hu et al.*, 2000] with exact computation of low orders of scattering [*Nakajima and Tanaka*, 1988]. The model

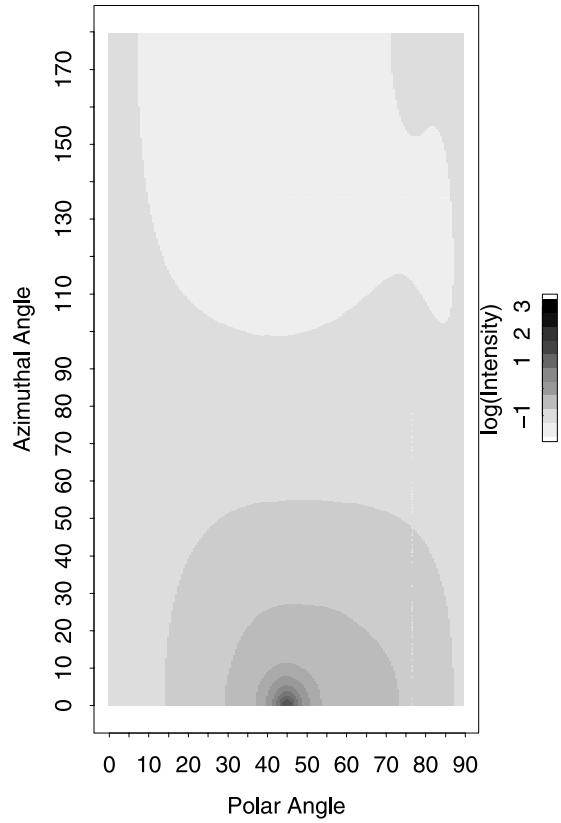

Figure 3. Simulated radiation intensity of water cloud with optical depth of 1 and effective radius of 8.5 μm.

can accurately and rapidly compute radiances in both forward and backward directions.

[9] In the following simulations, we use the Air Force Geophysics Laboratory (AFGL) midlatitude model and aerosol profile from MODTRAN [*Berk et al.*, 1989]. We divide the atmosphere into 20 layers and confine a water cloud layer at 1–2 km. To get accurate radiance, we use 64 streams in the Legendre polynomial expansion. An example of simulated radiation intensity of clouds is shown in Figure 3. In the simulation, the cloud optical depth is 1 with effective radius of 8 μm and the solar zenith angle is 45 degrees.

[10] To simulate MMR measurements, radiation intensities of various cloud conditions calculated by our fast radiative transfer model are blocked by the rotating shadowband strip at various blocking angles. We assume the shadow band blocks radiation with an umbral angle of 2 degrees and polar angles from 0 to 90 degrees. Figure 4a shows simulated MMR measurements as a function of blocking angles from 0 to 15 degree for 7 different effective radii. In this simulation, cloud optical depth and solar zenith angle are set to 1 and 45 degrees, respectively. Magnitudes of variation of blocked radiance (normalized intensity) for different effective radii are smaller than changes of the phase function because of the averaging effect of blocked area by the shadowband strip. However, the forward scattering lobe clearly varies with effective radius. As shown in Figure 4b, the small blocking angle corresponds to the large dynamic range of blocked radiance which is a function of effective radius. When the blocking angle is less than 5 degrees, changes of blocked radiance as a function of effective radius start to be detectable. From 5 degrees to about 1.4 degrees, the blocked radiance decreases with increase of effective radius. For a blocking angle less than 1.4 degrees, the blocked radiance increases with effective radius because of strong forward scattering of large cloud droplets. This demonstrates that the information of cloud particle size is contained within 5 degrees of the forward scattering lobe of the Sun.

[11] Figure 5 shows the blocked radiance as a function of cloud optical depth (equivalent to LWP for a given effective radius). In this case, we set the effective radius to be 8 μm with solar zenith angle of 45 degrees. The forward scattering lobe broadens with increase of cloud optical depth due to the enhancement of multiple scattering. As shown in Figure 5b, at zero blocking angle the blocked diffuse component into the field of view of MMR increases with increasing optical depth and reaches a maximum at an optical depth of 2.0, and then decreases. This is due to the combined effect of increase of scattering and an exponential decay of direct solar beam. The occurrence of the maximum blocked radiance shifts to higher optical depth with increasing blocking angle. Figures 4 and 5 demonstrate that both effective radius and optical depth (or LWP) can be simultaneously retrieved from the measurements of the forward scattering lobe of the solar aureole region.

3.2. Retrievals

[12] The blocked radiance, $F_i(\alpha_{sza}, \alpha_i, r_e, \tau)$, can be calculated by our forward radiative transfer model as a function of solar zenith angle, α_{sza}, blocking angle, α_i, effective radius, r_e, and optical depth, τ. For the measurements of forward scattering lobe, we have:

$$e_0 = b_0 - F_0(\alpha_{sza}, \alpha_0, r_e, \tau) - \exp(-\tau/\cos(\alpha_{sza}))$$
$$e_i = b_i - F_i(\alpha_{sza}, \alpha_i, r_e, \tau) \qquad i = \pm 1, \pm 2, \cdots, \pm m$$

where b_i and e_i are measured blocked radiance and error in the ith blocking angle, respectively. The MMR will scan across the sky from the right to the left of the Sun. For the Sun sensor direction ($\alpha_0 = 0$), the measured radiance contains both attenuated solar beam and forward scattering components. The effective radius and optical depth can be evaluated as the least squares minimum of the difference between the measured and modeled radiances in the above equation. On the basis of experience from multifilter rotating shadowband radiometers (MFRSR), the accuracy of the solar constant at a nongaseous absorption passband (wavelength channel) from the Langley regression calibration is within 1% [*Michalsky et al.*, 2001]. Therefore, in the following tests we set a random measurement error of 1%.

[13] Figure 6 shows simulated MMR measurements and fitting results based on our retrieval. In this case, the cloud effective radius and optical depth are set to be 8.5 μm and 1, respectively. The Sun is at 40 degrees of the zenith. The true values represent the measurements without errors; the measured values contain 1% random noise in the scan. The retrieval results are 8.42 μm and 1.004 for effective radius and optical depth, respective. The errors are less than 1% for both effective radius and optical depth.

[14] Tracking accuracy is an issue for the shadowband technique. Because of stepping error and possible misalignment of the polar axis, a shift in blocking angles may occur in the measurements. Therefore we assume an angular shifting

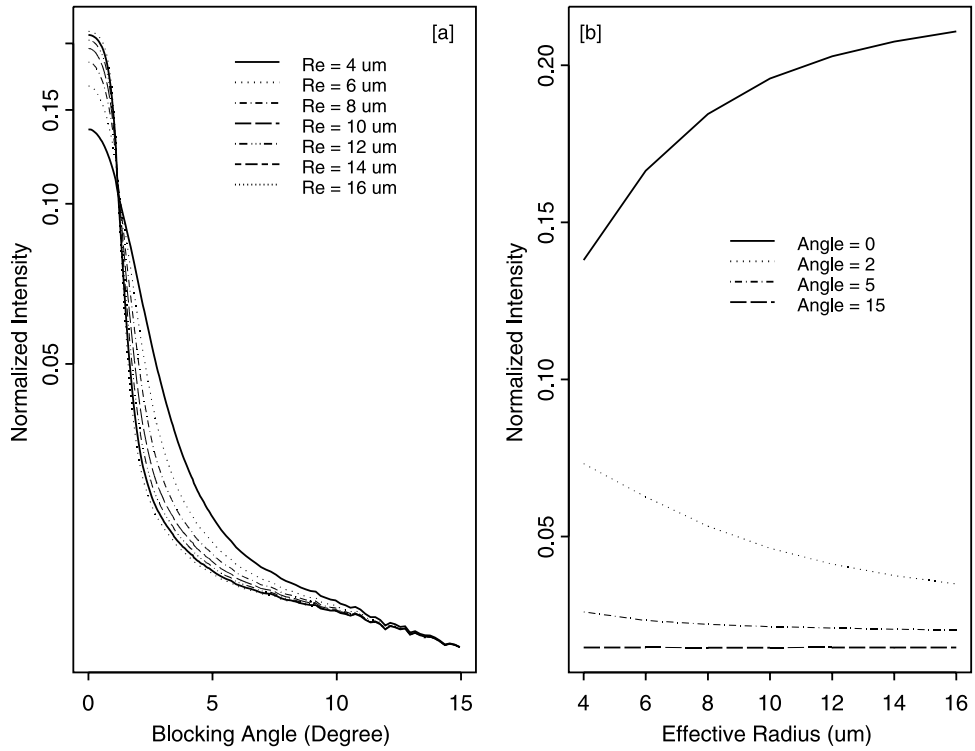

Figure 4. Simulated shadowband scans (normalized intensities) (a) as a function of blocking angles from 0 to 15 degree for 7 different effective radii and (b) as a function of cloud effective radius for blocking angles of 0, 2, 5 and 15 degree.

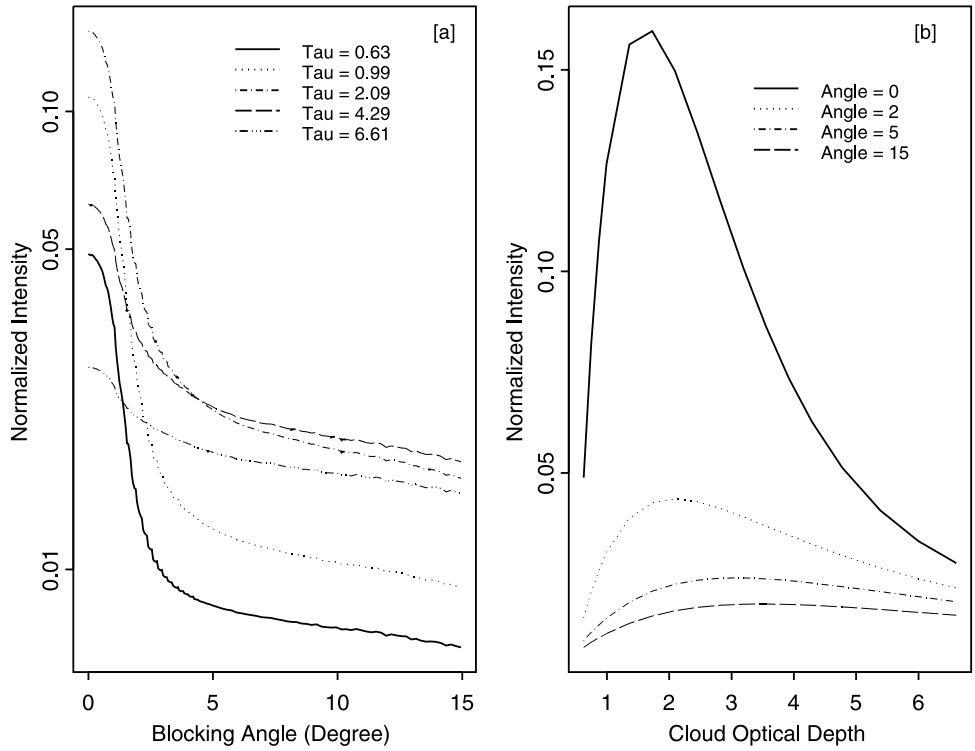

Figure 5. Simulated shadowband scans (normalized intensities) (a) as a function of blocking angles for different cloud optical depths and (b) as a function of cloud optical depth for blocking angles of 0, 2, 5 and 15 degree.

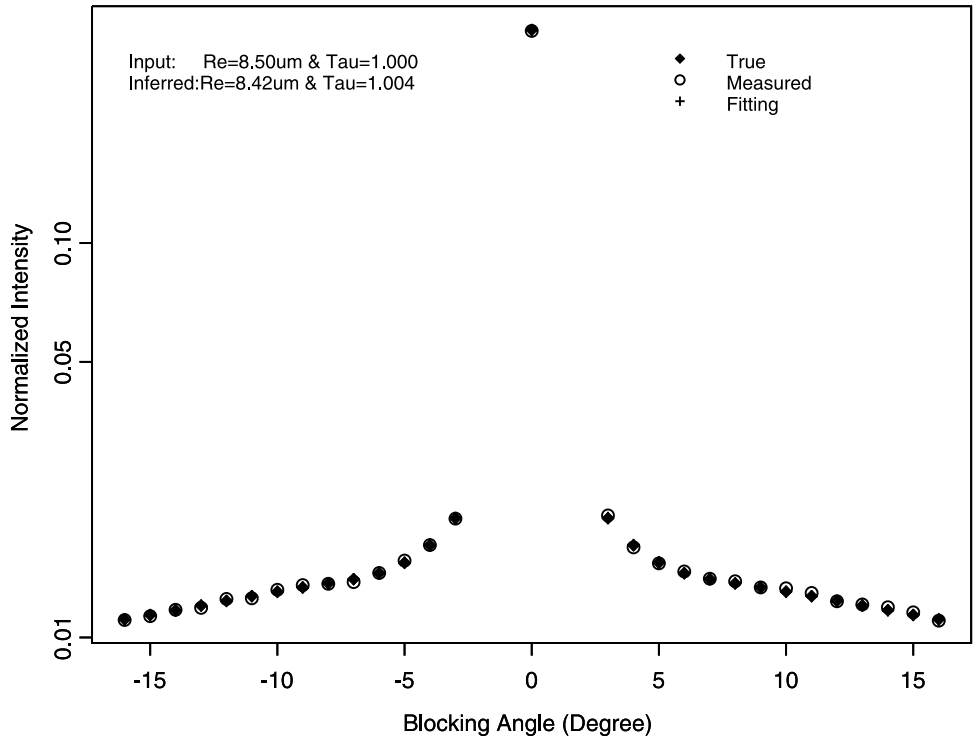

Figure 6. Simulated shadowband scan (normalized intensities) as a function of blocking angles. Solid diamonds represent modeled intensities without any uncertainty, open dots represent simulated measurements of MMR with 1% random errors, and plus signs represent final fitting results.

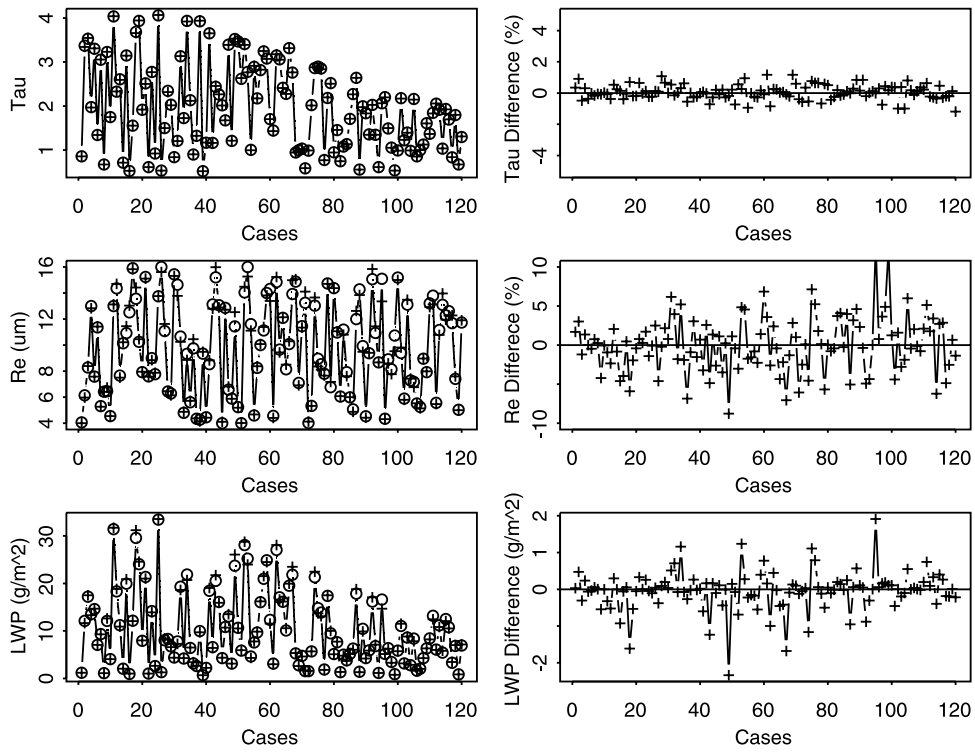

Figure 7. Comparison of cloud optical depth, effective radius, and LWP for 120 random cases between input values and retrieved results and their differences.

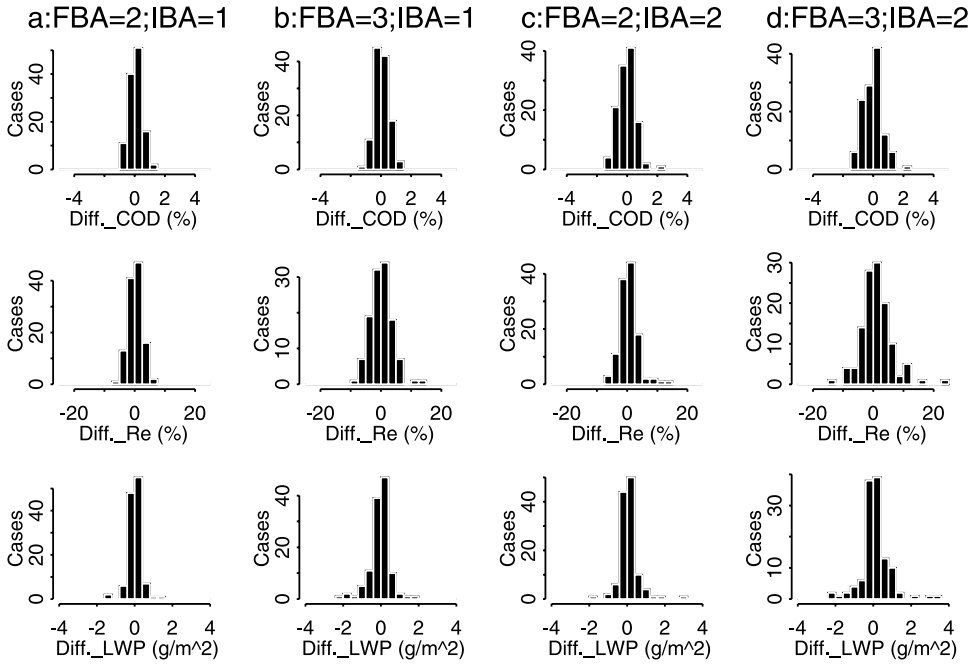

Figure 8. (a–d) Statistics of possible errors of retrieved optical depth, effective radius, and LWP for four different scan strategies. FBA and IBA stand for the first blocking angle and the incremental angle, respectively.

of 0.4 degrees with random noise of 2% in blocking angle in the scans in the following case. The setting for this case is the same as the previous case except for the blocking angle shifts. The retrieval results are 8.23 μm and 0.998 for effective radius and optical depth, respectively. The optical depth retrieval is less sensitive to the shift than the effective radius. The error for retrieving effective radius is up from 1% to 4%.

[15] To simulate real cloud scenes and test for a large range of conditions, we set up 120 random cases as our basic test. In these cases, the solar zenith angle changes from 25 to 70 degrees; the cloud optical depth and effective radius are randomly selected from 0 to 5 and from 4 to 16 μm, respectively. A random noise of 1% in radiometric error has been added to the measurements. As done previously, a random blocking angle shift with a maximum of 0.4 degrees is also applied to the measurements of each case. Figure 7 shows the comparison between input and retrieved optical depth and effective radius of cloud and their relative errors. In Figure 7, we also show the comparison of LWP calculated on the basis of optical depth and effective radius and their retrieval errors. The optical depth differences are less than 2% for all cases. The errors for retrieved effective radius are up to 10% with most cases under 5%. For the range of LWP up to 35 gm^{-2} the LWP differences are less than 2 gm^{-2}. It represents one order of magnitude improvement for retrieving LWP from MWR (20–30 gm^{-2}).

4. Instrument Design and Impacts

[16] Clouds change rapidly, requiring a fast scan across the solar aureole region to retrieve their properties. This in turn will affect the number of blocking measurements per scan. Further, the transmission diffuser of the inlet optic has a finite area. The diffuser, the width of shadowband strip, and rotating geometry would limit the umbral angle of the blocking band, and thus limit the first blocking angle away from the Sun sensor direction. We test four possible scan strategies using a first blocking angle of 2 or 3 degrees and an incremental blocking angle of 1 or 2 degrees (or equivalent to 29 and 15 steps of shadowband rotation). In each test, we set up 120 random cases with possible measurement uncertainties as discussed previously except for different first blocking angles and incremental angles. Figure 8 shows the statistics of possible errors of retrieved optical depth, effective radius, and LWP. Figure 8a, the first column, represents our basic test (see Figure 7). Sensitivity of the forward scattering radiance to the effective radius decreases as the blocking angle increases. If we change the first blocking angel to 3 degrees, as shown in Figure 8b, the errors of effective radius for most cases increase to 7% with few cases up to 15%. Meanwhile, the errors of optical depth increase slightly and are still less than 2%. The uncertainties of LWP retrievals are less than 2.2 gm^{-2}. If we reduce scanning steps by half, the errors of LWP retrievals increase to 3 gm^{-2} and 4 gm^{-2} for the first blocking angle of 2 or 3 degrees, respectively, as shown in Figures 8c and 8d. The increased errors are mainly due to increases in uncertainty of effective radius retrievals, as a consequence of fewer forward scattering lobe samples. Nonetheless, the error of LWP retrievals is much smaller than the retrievals from MWR.

5. Discussion and Summary

[17] We have proposed a new technique for simultaneously retrieving cloud optical depth and effective radius. This approach is based on the angular distribution of scattered

light in the forward scattering lobe of cloud drops in the solar aureole region. The angular distributions of the forward scattering lobe can be observed through multiple shadowband scans. Simulations demonstrate that accuracies for cloud optical depth, effective radius, and liquid water path are 2%, 10%, and 2 gm^{-2}, respectively for given possible instrument noise and uncertainties. This technique will fill current gaps in the accurate measurement of small cloud LWP.

[18] This technique can also be applied to the less challenging problem of retrieving aerosol optical depth and mean radius, since the forward scattering for relatively small aerosol particles is not as strong as for cloud droplets. Many previous retrieval approaches on the solar aureole are valid for proposed measurements. With the proposed MMR system (a multiple wavelength channels system), simultaneous spectral measurements of direct and diffuse transmittance would further enhance the capability of detecting aerosol and clouds. As described by *Min et al.* [2004], temporal and spectral variations (two channels at 415 and 860 nm) in direct beam radiation can be used to discriminate aerosol and very thin clouds. Furthermore, clouds and aerosols exhibit different angular characteristics in the forward scattering lobe. Aerosols and clouds can be discriminated and separated from temporal, spectral, and angular variations in the forward scattering lobe. Thus the contamination of aerosols in cloud retrievals can be minimized. With wavelength channels in ozone and water vapor absorption bands, this multichannel multiscan radiometer will be able to retrieve total amounts of ozone and water vapor in the atmosphere. More importantly, the measurements of forward scattering lobe will more accurately obtain the direct beam radiance by removing possible forward scattered radiance into the Sun sensor direction, resulting a more accurate retrieval of optical depths of various species (aerosol, cloud, ozone, and water vapor). Improved direct/diffuse radiation ratios can be used to derive aerosol single scattering albedo as well as to study radiation closure. The advantages of simultaneous measurements of forward scattering lobe (plus direct) and diffuse radiations using the same sensor would allow accurate calibration of both direct and diffuse radiation using Langley regression, and thus accurate atmospheric transmittance. The total diffuse transmittance will provide retrievals of cloud optical depth under thick cloud conditions when direct beam radiation is fully blocked by the cloud [*Min and Harrison*, 1996; *Min et al.*, 2003].

[19] **Acknowledgment.** This research was supported by the Office of Science (BER), U.S. Department of Energy, through the Atmospheric Radiation Measurement (ARM) grant DE-FG02-03ER63531, and through the Northeast Regional Center of the National Institute for Global Environmental Change (NIGEC) under Cooperative Agreement DE-FC03-90ER61010.

References

Barker, H., and A. Marshak (2001), Inferring optical depth of broken clouds above green vegetation using surface solar radiometer measurements, *J. Atmos. Sci.*, *58*, 2989–3006.

Berk, A., L. S. Bernstein, and D. C. Robertson (1989), MODTRAN: A moderate resolution model for LOWTRAN7, *Rep. AFGL-TR-89-0122*, Air Force Geophys. Lab., Hanscom Air Force Base, Mass.

Dong, X., T. P. Ackerman, E. E. Clothiaux, P. Pilewskie, and Y. Han (1997), Microphysical and radiative properties of boundary layer stratiform clouds deduced from ground-based measurements, *J. Geophys. Res.*, *102*, 23,829–23,843.

Dubovik, O., A. Smirnov, B. N. Holben, M. D. King, Y. J. Kaufman, T. F. Eck, and I. Slutsker (2000), Accuracy assessments of aerosol optical properties retrieved from Aerosol Robotic Network (AERONET) Sun and sky radiance measurements, *J. Geophys. Res.*, *105*, 9791–9806.

Hansen, J. E., and L. D. Travis (1974), Light scattering in planetary atmospheres, *Space Sci. Rev.*, *16*, 527–610.

Harrison, L. C., J. J. Michalsky, and J. Berndt (1994), Automated multifilter rotation shadowband radiometer: an instrument for optical depth and radiation measurements, *Appl. Opt.*, *33*, 5118–5125.

Hodkinson, J. R. (1966), Particle sizing by means of the forward scattering lobe, *Appl. Opt.*, *5*, 839–844.

Hu, Y. X., and K. Stamnes (1993), An accurate parameterization of the radiative properties of water clouds suitable for use in climate models, *J. Clim.*, *6*, 728–742.

Hu, Y.-X., B. Wielicki, B. Lin, G. Gibson, S.-C. Tsay, K. Stamnes, and T. Wong (2000), δ-Fit: A fast and accurate treatment of particle scattering phase functions with weighted singular-value decomposition least-squares fitting, *J. Quant. Spectrosc. Radiat. Transfer*, *65*, 681–690.

Kaufman, Y. J., A. Gitelson, A. Karnieli, E. Ganor, R. S. Fraser, T. Nakajima, S. Mattoo, and B. N. Holben (1994), Size distribution and scattering phase function of aerosol particles retrieved from sky brightness measurements, *J. Geophys. Res.*, *99*, 10,341–10,356.

Leontieva, E., and K. Stamnes (1996), Remote sensing of cloud optical properties from ground-based measurements of transmittance: A feasibility study, *J. Appl. Meteorol.*, *35*, 2011–2022.

Marchand, R., T. Ackerman, E. R. Westwater, S. A. Clough, K. Cady-Pereira, and J. C. Liljegren (2003), An assessment of microwave absorption models and retrievals of cloud liquid water using clear-sky data, *J. Geophys. Res.*, *108*(D24), 4773, doi:10.1029/2003JD003843.

Marshak, A., Y. Knyazikhan, A. B. Davis, W. J. Wiscombe, and P. Pilewskie (2000), Cloud-vegetation interaction: Using of normalized difference cloud index for estimation of cloud optical thickness, *Geophys. Res. Lett.*, *27*, 1695–1698.

Michalsky, J. J., J. A. Schlemmer, W. E. Berkheiser, J. L. Berndt, L. C. Harrison, N. S. Laulainen, N. R. Larson, and J. C. Barnard (2001), Multiyear measurements of aerosol optical depth in the atmospheric radiation measurement and quantitative links programs, *J. Geophys. Res.*, *107*, 12,099–12,107.

Min, Q.-L., and L. C. Harrison (1996), Cloud properties derived from surface MFRSR measurements and comparison with GOES results at the ARM SGP site, *Geophys. Res. Lett.*, *23*, 1641–1644.

Min, Q.-L., M. Duan, and R. Marchand (2003), Validation of surface retrieved cloud optical properties with in situ measurements at the Atmospheric Radiation Measurement Program (ARM) South Great Plains site, *J. Geophys. Res.*, *108*(D17), 4547, doi:10.1029/2003JD003385.

Min, Q.-L., E. Joseph, and M. Duan (2004), Retrievals of thin cloud optical depth from a multifilter rotating shadowband radiometer, *J. Geophys. Res.*, *109*, D02201, doi:10.1029/2003JD003964.

Min, Q.-L., M. Duan, L. C. Harrison, and E. Joseph (2005), A decade-long aerosol and cloud statistics and aerosol indirect effect at the ARM SGP site, paper presented at ARM Science Team Meeting, Daytona Beach, Fla.

Nakajima, T., and M. Tanaka (1988), Algorithms for radiative intensity calculations in moderately thick atmospheres using a truncation approximation, *J. Quant. Spectrosc. Radiat. Transfer*, *40*, 51–69.

Nakajima, T., M. Tanaka, and T. Yamauchi (1983), Retrieval of the optical properties of aerosols from aureole and extinction data, *Appl. Opt.*, *22*, 2952–2959.

Ritter, J. M., and K. J. Voss (2000), A new instrument for measurement of the solar aureole radiance distribution from unstable platforms, *J. Atmos. Oceanic Technol.*, *17*, 1040–1048.

Stamnes, K., S.-C. Tsay, W. J. Wiscombe, and K. Jayaweera (1988), Numerical stable algorithm for discrete-ordinate-method radiative transfer in multiple scattering and emitting layered media, *Appl. Opt.*, *27*, 2502–2509.

Wiscombe, W. J. (1977), Delta-M method: Rapid yet accurate radiative flux calculations for strongly asymmetric phase functions, *J. Atmos. Sci.*, *34*(9), 1408–1422.

M. Duan and Q. Min, Atmospheric Science Research Center, State University of New York, Albany, NY 12203, USA. (min@asrc.cestm.albany.edu)